Nonlinear model for Galfenol cantilevered unimorphs considering full magnetoelastic coupling

Liang Shu[1,2], Leon M Headings[2], Marcelo J Dapino[2], Dingfang Chen[3] and Quanguo Lu[4]

Abstract
This article presents a fully coupled, nonlinear model for the dynamic response of Galfenol-driven unimorph actuators in a cantilever configuration. The hysteretic magnetomechanical behavior of Galfenol is modeled using a discrete energy-averaged model, and the structural behavior of the unimorph is modeled using the finite element method. The weak form equations that describe bending of the unimorph are obtained using the principle of virtual work. Since the local strain and stress are nonlinearly coupled with both the vertical and horizontal displacements, a nonlinear solver is developed to approximate the coupled finite element equations. The nonlinear solver is verified against the analytical solution and experimental data for the case of a passive beam. The analytical solution is obtained using beam theory for free and harmonic responses. The analytical model and experimental data verify that the nonlinear solver correctly quantifies the first natural frequency of the composite beam. The numerical simulations match the analytical solutions for both free and harmonic responses. Finally, the dynamic response of the nonlinear magnetoelastic model is investigated and experimentally validated from 0.1 to 500 Hz, the range in which the model is accurate without the need for adjustable parameters.

Introduction

Galfenol is a magnetostrictive material which can be safely operated in tension, compression, and shear (Evans and Dapino, 2008). Due to their ability to operate in large deformation regimes without special treatments, laminated bender structures utilizing Galfenol drivers provide an attractive alternative to brittle materials like lead zirconate titanate (PZT) and Terfenol-D (Baillargeon and Vel, 2005; Shu et al., 2010). Wang et al. (2010) proposed a magnetoelectric cantilever composed of a layer of Galfenol and a layer of PZT-5H. This configuration offers advantages for potential use in microsurgical ablation tools and cutting tools for machining. Ueno and Higuchi (2008) presented a 2-degree-of-freedom (DOF) microbending actuator driven with Galfenol. An arrangement of orthogonal–parallel Galfenol beams creates bending deformation in both the *x*- and *y*-directions. Basantkumar et al. (2006) developed a microelectromechanical system (MEMS) actuator by integrating thin-film Galfenol with glass cover slides. Using a capacitance technique, the saturation magnetostriction of the film was measured to be 147 ppm (parts per million). Downey and Flatau (2005) investigated the magnetoelastic bending of Galfenol for sensor applications. When a sinusoidal load was applied to both polycrystalline and single-crystal rods, the magnetic induction was found to increase with applied magnetic bias.

[1]The Key Laboratory of Low-Voltage Apparatus Intellectual Technology of Zhejiang, Wenzhou University, Wenzhou, China
[2]Department of Mechanical and Aerospace Engineering, The Ohio State University, Columbus, OH, USA
[3]School of Logistics Engineering, Wuhan University of Technology, Wuhan, China
[4]School of Mechanical and Electrical Engineering, Nanchang Institutite of Technology, Nanchang, China

Corresponding author:
Marcelo J Dapino, Department of Mechanical and Aerospace Engineering, The Ohio State University, E307 Scott Laboratory, 201 West 19th Avenue, Columbus, OH 43210, USA.
Email: dapino.1@osu.edu

To investigate the structural and magnetoelastic coupling in laminated Galfenol benders, advanced models are required. Models for magnetostriction-induced represent one class of advanced models in which tip deflection is investigated in terms of magnetostriction, thickness ratio, and elastic properties (Du Tremolet de Lacheisserie and Peuzin, 1994; Gehring et al., 2000; Guerrero and Wetherhold, 2003; Quandt and Ludwig, 2000). Du Tremolet de Lacheisserie and Peuzin (1994) investigated the deformation of a bimorph consisting of a nonmagnetic substrate and a magnetic thin film. Their model is formulated for a thin film deposited on a nonmagnetic substrate. Since the film thickness is assumed to be much smaller than the substrate thickness, the internal stress in the film changes very little throughout the thickness, and the mechanical energy in the active layer can be assumed to be constant. Models that can be applied to any thickness ratio have been presented by Gehring et al. (2000) and Guerrero and Wetherhold (2003) based on total internal energy minimization. However, these models assume that the magnetostriction of the active layer is known a priori. The nonlinear stress and field dependency of the magnetoelastic processes in the structural bending cannot be quantified.

Other models aim to determine magnetomechanical coupling from magnetostriction-induced bending. A nonlinear optimal control strategy is presented by Smith (1998) in which a nonlinear magnetostrictive actuator model is developed to attenuate transverse beam vibrations. The linear Euler–Bernoulli equation is employed to model the structural bending of the cantilever. Jia et al. (2006) developed a nonlinear model to characterize the magnetization and magnetostriction processes of bimorph films. However, the change of internal stress during magnetization and magnetostriction is neglected, making the model accurate only for low magnetic fields. Datta et al. (2008) developed a magnetomechanical model for sensors in laminated plates. This model can be used to analyze the response of the active Galfenol layer to quasi-static axial and shear forces and bending moments. An actuation model was proposed by Datta et al. (2009) to describe magnetostrictive strains and stress in laminated plates under quasi-static magnetic fields. The contribution of this work was the combination of the magnetomechanical material model with the plate structural model for laminated structures; however, it cannot be used to examine the dynamic response of the system. A bidirectionally coupled magnetoelastic model was developed by Mudivarthi et al. (2008) in which the Armstrong model was combined with finite element elastic and magnetic models. The model describes material responses considering the spatial variation in magnetic field and stress. To investigate the dynamics of laminated structures with intrinsic magnetomechanical coupling, a nonlinear model that accounts for dynamic response together with the nonlinear stress and field dependency of magnetostriction is required.

This article addresses the dynamic response of Galfenol-driven cantilevered unimorphs. A discrete energy-averaged model is employed to describe the hysteretic magnetomechanical behavior of Galfenol, and the finite element method is used to model the structural behavior of the beam. Since the finite element model is time dependent, this model offers the advantage of solving dynamic problems in active laminated structures. The structural model is implemented in two dimensions (2D) by expressing the strain in terms of horizontal and vertical displacements. A discrete energy-averaged model is used to quantify the magnetostriction as a function of induced stress and field, both of which are simultaneously coupled with output displacements. In order to solve the nonlinear coupled equations, a numerical solver is developed to solve for vertical and horizontal displacements. The nonlinear stress and field dependency of magnetostriction is investigated, and experimental validation is conducted over the frequency range of 0.1–500 Hz. Simulation and experimental results show that the proposed model can predict the first natural frequency of the composite beam.

Composite beam model

Geometric considerations

A composite beam consisting of a Galfenol layer bonded to a nonmagnetic substrate is clamped at one end, while the other end is free (Figure 1). The $x - y$ plane of the coordinate system is set on the midplane of the cantilever; the z-axis is perpendicular to the active layer. The beam has length L and width b; the Galfenol layer has thickness t_g, modulus E_g, and density ρ_g and is assumed to be perfectly bonded to the substrate of thickness t_s, modulus E_s, and density ρ_s.

Principle of virtual work

When a magnetic field H is applied along x, the magnetostriction induces bending of the cantilever. The stress in the substrate σ_s is assumed to behave in a linearly elastic fashion relative to the strain ε_s, $\sigma_s = E_s \varepsilon_s$. The total strain induced in the Galfenol layer ε_g is assumed to consist of a magnetostrictive component superimposed on the elastic response of the material. The internal stress in the Galfenol layer can thus be expressed as

$$\sigma_g = E_g \left[\varepsilon_g - \lambda \left(\sigma_g, H \right) \right] \tag{1}$$

where the magnetostriction $\lambda \left(\sigma_g, H \right)$ depends on both internal stress and magnetic field. For the magnetostriction-induced bending, the total strain is the superposition of the extensional and bending strains

$$\varepsilon = \frac{\partial u(t, x)}{\partial x} - z \frac{\partial^2 v(t, x)}{\partial x^2}. \tag{2}$$
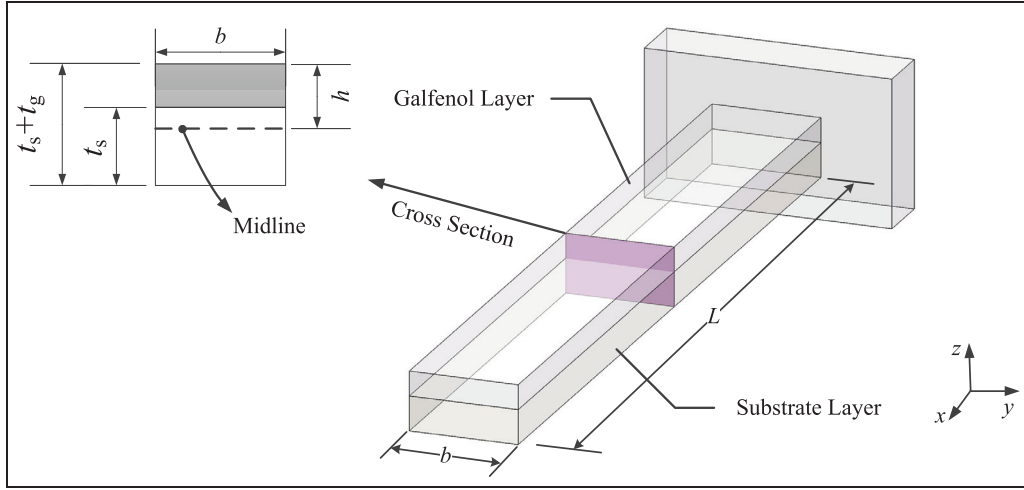
Figure 1. Beam geometry and coordinate system used to describe the cantilevered unimorph. An axial magnetic field applied to the Galfenol layer induces bending of the cantilever.

Here, $u(t,x)$ denotes the horizontal displacement of the midplane and $v(t,x)$ denotes the vertical displacement. The principle of virtual work is considered in order to relate the magnetostriction to the horizontal and vertical displacements. Recognizing that the external virtual work is zero when no external load is applied, one obtains

$$-\delta W_i - \delta W_e = -\delta W_i = 0. \tag{3}$$

The subscripts i and e denote internal and external components of the virtual work, respectively. The internal virtual work arises from internal stress, dynamic inertia, and damping effects. The virtual work from stress has the following form (see Appendix 1)

$$\delta W_\sigma = \int_0^L \int_A \sigma \delta\varepsilon \, dA \, dx$$

$$= \int_0^L \int_{A_g} \sigma_g \delta\varepsilon_g \, dA_g \, dx + \int_0^L \int_{A_s} \sigma_s \delta\varepsilon_s \, dA_s \, dx$$

$$= E_g I_g \int_0^L \frac{\partial^2 v(t,x)}{\partial x^2} \delta \frac{\partial^2 v(t,x)}{\partial x^2} dx - E_g Q_g \int_0^L \frac{\partial^2 v(t,x)}{\partial x^2} \delta \frac{\partial u(t,x)}{\partial x} dx$$

$$- E_g Q_g \int_0^L \frac{\partial u(t,x)}{\partial x} \delta \frac{\partial^2 v(t,x)}{\partial x^2} dx + E_g A_g \int_0^L \frac{\partial u(t,x)}{\partial x} \delta \frac{\partial u(t,x)}{\partial x} dx$$

$$+ E_g \int_0^L \int_{A_g} \lambda \delta \frac{\partial^2 v(t,x)}{\partial x^2} z \, dA_g \, dx - E_g \int_0^L \int_{A_g} \lambda \delta \frac{\partial u(t,x)}{\partial x} dA_g \, dx$$

$$+ E_s I_s \int_0^L \frac{\partial^2 v(t,x)}{\partial x^2} \delta \frac{\partial^2 v(t,x)}{\partial x^2} dx - E_s Q_s \int_0^L \frac{\partial^2 v(t,x)}{\partial x^2} \delta \frac{\partial u(t,x)}{\partial x} dx$$

$$- E_s Q_s \int_0^L \frac{\partial u(t,x)}{\partial x} \delta \frac{\partial^2 v(t,x)}{\partial x^2} dx + E_s A_s \int_0^L \frac{\partial u(t,x)}{\partial x} \delta \frac{\partial u(t,x)}{\partial x} dx$$

$$\tag{4}$$

In order to calculate the internal virtual work from dynamic inertia, the d'Alembert force, which is a function of the horizontal and vertical accelerations is considered. Also, Kelvin–Voigt damping, a function of the horizontal and vertical velocities, is employed to calculate the internal virtual work from damping effects

$$\delta W_\rho = \int_0^L \int_A \rho \frac{\partial^2 u(t,x)}{\partial t^2} \delta u \, dA \, dx + \int_0^L \int_A \rho \frac{\partial^2 v(t,x)}{\partial t^2} \delta v \, dA \, dx$$

$$\delta W_c = \int_0^L \int_A c \frac{\partial u(t,x)}{\partial t} \delta u \, dA \, dx + \int_0^L \int_A c \frac{\partial v(t,x)}{\partial t} \delta v \, dA \, dx$$

$$\tag{5}$$

where the subscripts ρ and c denote virtual work from inertia and damping, respectively. The weak form equation of the magnetostriction-induced bending is therefore given as follows

$$E_g I_g \int_0^L \frac{\partial^2 v(t,x)}{\partial x^2} \delta \frac{\partial^2 v(t,x)}{\partial x^2} dx - E_g Q_g \int_0^L \frac{\partial^2 v(t,x)}{\partial x^2} \delta \frac{\partial u(t,x)}{\partial x} dx$$

$$- E_g Q_g \int_0^L \frac{\partial u(t,x)}{\partial x} \delta \frac{\partial^2 v(t,x)}{\partial x^2} dx + E_g A_g \int_0^L \frac{\partial u(t,x)}{\partial x} \delta \frac{\partial u(t,x)}{\partial x} dx$$

$$+ E_s I_s \int_0^L \frac{\partial^2 v(t,x)}{\partial x^2} \delta \frac{\partial^2 v(t,x)}{\partial x^2} dx - E_s Q_s \int_0^L \frac{\partial^2 v(t,x)}{\partial x^2} \delta \frac{\partial u(t,x)}{\partial x} dx$$

$$- E_s Q_s \int_0^L \frac{\partial u(t,x)}{\partial x} \delta \frac{\partial^2 v(t,x)}{\partial x^2} dx + E_s A_s \int_0^L \frac{\partial u(t,x)}{\partial x} \delta \frac{\partial u(t,x)}{\partial x} dx$$

$$+ \int_0^L \int_A \rho \frac{\partial^2 u(t,x)}{\partial t^2} \delta u \, dA \, dx + \int_0^L \int_A \rho \frac{\partial^2 v(t,x)}{\partial t^2} \delta v \, dA \, dx$$

$$+ \int_0^L \int_A c \frac{\partial u(t,x)}{\partial t} \delta u \, dA \, dx + \int_0^L \int_A c \frac{\partial v(t,x)}{\partial t} \delta v \, dA \, dx$$

$$= - E_g \int_0^L \int_{A_g} \lambda \delta \frac{\partial^2 v(t,x)}{\partial x^2} z \, dA_g \, dx + E_g \int_0^L \int_{A_g} \lambda \delta \frac{\partial u(t,x)}{\partial x} \, dA_g \, dx$$

$$(6)$$

It can be seen from equation (6) that both $u(t,x)$ and $v(t,x)$ depend on $\lambda(\sigma_g, H)$. From equations (1) and (2), the internal stress σ can be seen to also depend on the output displacements $u(t,x)$ and $v(t,x)$. These equations describe the nonlinear coupling in magnetostriction-induced. In order to solve for $u(t,x)$ and $v(t,x)$ from equation (6), the weak form equation is discretized in the spatial domain.

Finite element discretization

The beam is discretized into N_e elements of length l_e, each with two nodes, for a total of $N_n = N_e + 1$ nodes (see Figure 2(a)). Each node has 3 DOFs. The first two are vertical displacement $v(t,x)$ and rotation $\partial v(t,x)/\partial x$, which contribute a total of $N_q^v = 2N_n$ DOFs to the discretized beam; the other nodal DOF is horizontal displacement $u(t,x)$, which contributes a total of $N_q^u = N_n$ DOFs. The values of the DOFs associated with the vertical displacement for a single element are denoted as $\mathbf{q}_e^v$, in which the first two components are the vertical displacement and rotation of the left node and the second two are the vertical displacement and rotation of the right node. The global notation is $\mathbf{Q}^v$. The values of the DOFs associated with the horizontal displacement for a single element are denoted as $\mathbf{q}_e^u$, where the first entry is the horizontal displacement of the left node and

the second entry is the horizontal displacement of the right node. The global notation is $\mathbf{Q}^u$.

Hermite shape functions are chosen to ensure the continuity of $v(t,x)$ and $\partial v(t,x)/\partial x$. The local spatial coordinate is taken as ξ, ranging from -1 to 1, and the vertical displacement is interpolated as follows

$$v_e = \mathbf{H} \cdot \mathbf{q}_e^v = \left[H_1, \frac{l_e}{2} H_2, H_3, \frac{l_e}{2} H_4 \right] \left[q_{e,1}^v, q_{e,2}^v, q_{e,3}^v, q_{e,4}^v \right]^\top$$

$$(7)$$

where $\mathbf{H}$ is the shape function vector. The horizontal displacement requires only continuity of the zeroth derivative. Linear shape functions are chosen, and the horizontal displacement is interpolated as follows

$$u_e = \mathbf{N} \cdot \mathbf{q}_e^u = [N_1, N_2] \left[q_{e,1}^u, \ q_{e,2}^u \right]^\top \qquad (8)$$

where $\mathbf{N}$ is the linear shape function vector. The components of $\mathbf{H}$ and $\mathbf{N}$ are shown in Appendix 2. The discretized weak form equation can be obtained by substituting equations (7) and (8) into equation (6) (see Appendix 2 for details)

$$\sum_e \{\mathbf{q}_e^v\}^\top \cdot [\mathbf{k}_e^v] \{\delta \mathbf{q}_e^v\} - \{\mathbf{q}_e^v\}^\top \cdot [\mathbf{k}_e^{uv}] \{\delta \mathbf{q}_e^u\}$$

$$- \{\mathbf{q}_e^u\}^\top \cdot [\mathbf{k}_e^{uv}]^\top \{\delta \mathbf{q}_e^v\} + \{\mathbf{q}_e^u\}^\top \cdot [\mathbf{k}_e^u] \{\delta \mathbf{q}_e^u\}$$

$$+ \sum_e \{\ddot{\mathbf{q}}_e^u\}^\top \cdot [\mathbf{m}_e^u] \{\delta \mathbf{q}_e^u\} + \{\ddot{\mathbf{q}}_e^v\}^\top \cdot [\mathbf{m}_e^v] \{\delta \mathbf{q}_e^v\}$$

$$+ \sum_e \{\dot{\mathbf{q}}_e^u\}^\top \cdot [\mathbf{c}_e^u] \{\delta \mathbf{q}_e^u\} + \{\dot{\mathbf{q}}_e^v\}^\top \cdot [\mathbf{c}_e^v] \{\delta \mathbf{q}_e^v\}$$

$$= \sum_e - [\mathbf{f}_e^{\lambda, v}] \{\delta \mathbf{q}_e^v\} + [\mathbf{f}_e^{\lambda, u}] \{\delta \mathbf{q}_e^u\}$$

$$(9)$$

Applying variational principles, the assembled system to be solved is

$$[\mathbf{M}]\{\ddot{\mathbf{Q}}^{uv}\} + [\mathbf{C}]\{\dot{\mathbf{Q}}^{uv}\} + [\mathbf{K}]\{\mathbf{Q}^{uv}\} = \left[\mathbf{F}_\lambda^{uv}\right] \qquad (10)$$

where

$$[\mathbf{M}] = \begin{bmatrix} \mathbf{m}_e^u & 0 \\ 0 & \mathbf{m}_e^v \end{bmatrix}, \quad [\mathbf{C}] = \begin{bmatrix} \mathbf{c}_e^u & 0 \\ 0 & \mathbf{c}_e^v \end{bmatrix},$$

$$[\mathbf{K}] = \begin{bmatrix} \mathbf{k}_e^u & -(\mathbf{k}_e^{uv})^\top \\ -(\mathbf{k}_e^{uv}) & \mathbf{k}_e^v \end{bmatrix}, \quad \left[\mathbf{F}_\lambda^{uv}\right] = \begin{bmatrix} \mathbf{f}_e^{\lambda, u} \\ -\mathbf{f}_e^{\lambda, v} \end{bmatrix},$$

$$\{\mathbf{Q}^{uv}\} = \begin{bmatrix} \mathbf{q}_e^u \\ \mathbf{q}_e^v \end{bmatrix}$$

It is seen in equation (10) that the global mass matrix $[\mathbf{M}]$ and the global damping matrix $[\mathbf{C}]$ are diagonal, which is consistent with the d'Alembert force and Kelvin–Voigt damping considered here since induced forces are proportional to the mass and damping. The stiffness matrix $[\mathbf{K}]$ is nondiagonal because the internal stress is coupled with both the vertical and horizontal
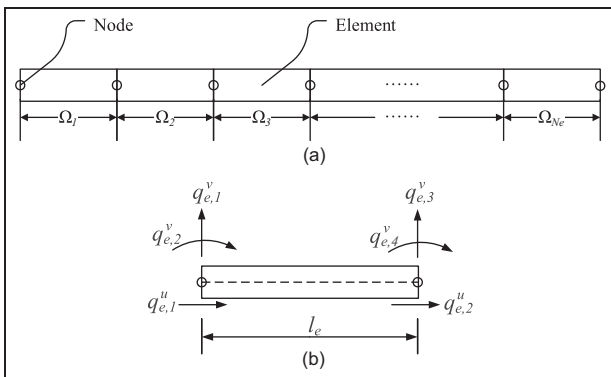

Figure 2. (a) Discretization of the beam and (b) degrees of freedom of an element.

displacements. Array $\{\mathbf{Q}^{uv}\}$ is the generalized displacement, while $\{\dot{\mathbf{Q}}^{uv}\}$ and $\{\ddot{\mathbf{Q}}^{uv}\}$ denote the generalized velocity and acceleration, respectively. The excitation vector $\left[\mathbf{F}_{\lambda}^{uv}\right]$ is a function of the magnetostriction, which depends on the induced strain and stress in the actuator. This creates nonlinear coupling in the magnetoelastic process. Furthermore, since inertial and damping effects are considered, this model can be used to solve dynamic problems in laminated structures. The general framework developed here can also be applied to other dynamic magnetomechanical coupling problems.

Three-dimensional hysteretic constitutive law

The magnetostriction induced by the Galfenol element must be known to solve for the state variable $\{\mathbf{Q}^{uv}\}$. In order to account for field and stress dependency, a discrete energy-averaged model (Evans and Dapino, 2010) is employed to describe the hysteretic magnetomechanical behavior of Galfenol. This model improves recent work (Zhou and Zhou, 2007), in which only anhysteretic responses were considered in the active layer of a laminated structure. This work was limited to one-dimensional (1D) analysis and did not account for magnetocrystalline anisotropy. In the discrete energy-averaged model, local anisotropy energy is defined, and three-dimensional (3D) magnetomechanical rsponses are described through minimization of the total free energy of Galfenol. Hysteresis is considered by formulating the evolution equation of volume fraction in terms of both stress and magnetic field. For a material composed of a collection of Stoner–Wohlfarth (SW) particles (Stoner and Wohlfarth, 1948) in thermodynamic equilibrium and having r possible orientations, the bulk magnetostriction $\boldsymbol{\lambda}$ is the sum of the magnetostriction $\boldsymbol{\lambda}^i$ in each direction, weighted by the volume fraction ζ^i of particles in each orientation

$$\boldsymbol{\lambda} = \sum_{i=1}^{r} \boldsymbol{\lambda}^i(\mathbf{m}^i)\zeta^i, \qquad (11)$$

where $\mathbf{m}^i$ represents the magnetic orientations of the SW particles. Rather than use a globally defined energy expression and sum over all possible orientations (Atulasimha et al., 2008), Evans and Dapino (2010) defined the energy around local energy minima corresponding to the easy crystallographic directions. Only the local minima are included in the summation. For cubic materials, these directions are typically the 6 $\langle 100 \rangle$ directions or 8 $\langle 111 \rangle$ directions or both sets together for a total of 14 directions. The anisotropy energy for these directions is analogous to a mechanical spring with initial configuration $\mathbf{m}_0^i$ (corresponding to the easy crystallographic directions) and stiffness represented by the anisotropy coefficient K^i. In cubic materials, all the $\langle 100 \rangle$ directions have the same coefficient, $K^i = K_{100}$, as do the $\langle 111 \rangle$ directions, $K^i = K_{111}$.

The local energy for each minimum $\mathbf{m}^i$ therefore has the following form

$$E^i = \tfrac{1}{2}K^i\left|\mathbf{m}^i - \mathbf{m}_0^i\right|^2 - \boldsymbol{\lambda}(\mathbf{m}^i) \cdot \mathbf{T} - \mu_0 M_S \mathbf{m}^i \cdot \mathbf{H} \quad (12)$$

where $\mathbf{T}$ is the internal stress tensor, $\mathbf{H}$ is the applied field, and M_S is the saturation magnetization. The magnetic orientations $\mathbf{m}^i$ can be calculated by minimization of the total free energy (12) with the constraint $C = |\mathbf{m}^i| - 1 = 0$ (since $\mathbf{m}^i$ is a unit vector). In order to solve for $\mathbf{m}^i$ analytically, the constraint is relaxed through linearization about the easy direction $\mathbf{m}_0^i$ by assuming $\mathbf{m}_0^i \cdot \mathbf{m}^i \approx \mathbf{m}^i \cdot \mathbf{m}^i = 1$. The solution for the magnetic orientations is

$$\mathbf{m}^i = \left(\mathbf{K}^i\right)^{-1}\left[\mathbf{B}^i + \left(\frac{1 - \mathbf{m}_0^i \cdot (\mathbf{K}^i)^{-1}\mathbf{B}^i}{\mathbf{m}_0^i \cdot (\mathbf{K}^i)^{-1}\mathbf{m}_0^i}\right)\mathbf{m}_0^i\right], \qquad (13)$$

where $\mathbf{K}^i$ is the magnetic stiffness matrix and $\mathbf{B}^i$ is a force vector

$$\begin{aligned}
\mathbf{B}^i &= K^i\mathbf{m}^i + \mu_0 M_S\mathbf{H}, \\
\mathbf{K}^i &= \begin{bmatrix} K^i - 3\lambda_{100}T_1 & -3\lambda_{111}T_4 & -3\lambda_{111}T_6 \\ -3\lambda_{111}T_4 & K^i - 3\lambda_{100}T_2 & -3\lambda_{111}T_5 \\ -3\lambda_{111}T_6 & -3\lambda_{111}T_5 & K^i - 3\lambda_{100}T_3 \end{bmatrix}.
\end{aligned}$$

This solution assumes that domains rotate a small angle away from the easy directions. The error associated with this assumption is very small since particles that have rotated far from the easy axes have much smaller volume fractions than particles that have not rotated far. Thus, the magnetostriction calculated from equation (11) mostly depends on the particles that are relatively close to the easy directions. In order to calculate the magnetostriction, the volume fraction ζ^i must be quantified.

Armstrong (2003) proposed an evolution law for a unidirectional applied field

$$\Delta\zeta^i = \tfrac{1}{k}\left(\zeta_{an}^i - \zeta^i\right)|\Delta H|, \qquad (14)$$

in which hysteresis arises from energy losses as domain walls overcome pinning sites. This model only explains hysteresis when the magnetic field is varied at constant stress and only applies to one-dimensional problems. Since both stress and field change the domain volume fractions through domain wall rotation, the irreversible changes of volume fractions due to 3D magnetic field and stress are

$$\begin{aligned}
\Delta\zeta_{irr}^i = \frac{1}{k}\left(\zeta_{an}^i - \zeta^i\right)&\left[\mu_0 M_S \sum_{i=1}^{3}\Delta H_i + \frac{3}{2}\lambda_{100}\right. \\
&\left. \sum_{i=1}^{3}\Delta T_i + 3\lambda_{111}\sum_{i=4}^{6}\Delta T_i\right],
\end{aligned} \qquad (15)$$

where k is a pinning site density constant that characterizes the energy loss associated with domain wall

rotation. The anhysteretic value of the volume fraction ζ^i_{an} can be calculated using an energy-weighted average,

$$\zeta^i_{an} = \frac{e^{-E^i/\Omega_s}}{\sum\limits_{i=1}^{r} e^{-E^i/\Omega_s}}, \qquad (16)$$

where Ω_s is a smoothing factor and E^i is the free energy associated with orientation $\mathbf{m}^i$. Following the theory by Jiles and Atherton (1986), the total increment in volume fraction is the sum of reversible and irreversible components

$$\Delta\zeta^i = c\Delta\zeta^i_{an} + (1-c)\Delta\zeta^i_{irr}, \qquad (17)$$

where c is a nondimensional constant which quantifies the reversible processes during domain wall motion. If $c = 1$, the total volume fraction corresponds to reversible processes ($\Delta\zeta^i = \Delta\zeta^i_{an}$), whereas if $c = 0$, the domain processes are fully irreversible ($\Delta\zeta^i = \Delta\zeta^i_{irr}$).

Unidirectional, hysteretic constitutive law

The magnetostriction expression (11) is 3D. In order to apply equation (11) to unidirectional bending, a unidirectional constitutive law is needed. Assume that a magnetic field or stress is applied in the direction u with respect to the crystal frame. Then, the auxiliary vector $\mathbf{u_T} = [u_1^2 \ u_2^2 \ u_3^2 \ u_1u_2 \ u_2u_3 \ u_3u_1]^\top$ relates the 3D magnetostriction to the longitudinal component λ^i in the application direction

$$\lambda^i = \mathbf{u}_\sigma \cdot \boldsymbol{\lambda}^i = \frac{1}{2}\mathbf{m}^i \cdot \mathbf{R} \cdot \mathbf{m}^i \qquad (18)$$

where

$$\mathbf{R} = 3\begin{bmatrix} \lambda_{100}u_{\sigma,1} & \lambda_{111}u_{\sigma,4} & \lambda_{111}u_{\sigma,6} \\ \lambda_{111}u_{\sigma,4} & \lambda_{100}u_{\sigma,2} & \lambda_{111}u_{\sigma,5} \\ \lambda_{111}u_{\sigma,6} & \lambda_{111}u_{\sigma,5} & \lambda_{100}u_{\sigma,3} \end{bmatrix}$$

so that the bulk unidirectional magnetostriction is represented as follows

$$\lambda = \sum_{i=1}^{r} \lambda^i \zeta^i. \qquad (19)$$

Simulation results of the hysteresis model are shown in Figure 3 for both completely reversible and irreversible processes. When $c = 0$, there is a stress-dependent hysteresis between strain and the applied field (Figure 3(a)). Since the whole process is completely irreversible, this hysteresis is quantified by the pinning site density. When $c = 1$, the behavior between strain and field becomes anhysteretic (Figure 3(b)), and the magnetostriction process is fully reversible. The induced strain due to varying stress is investigated in Figure 3(c) and (d), in which volume fractions are calculated from equations (14) and (15), respectively. It can be seen

from Figure 3(c) that the induced strain is linear with stress, with the slope representing the material's compliance. The model represented by equation (14) does not account for hysteresis when stress is varied at a constant field. Furthermore, the four plot lines representing different constant bias fields overlap, meaning that this model also does not account for the influence of bias field. Hysteresis is observed in Figure 3(d) for the model represented by equation (15). It can be seen that the slopes in the hysteretic regions are different at different bias fields, consistent with the ΔE effect. The linear regions are due to the dead zone and saturation of magnetization. When the magnetization does not change, the strain versus stress relationship is only governed by Hooke's law.

Numerical approximation

Since equation (10) is nonlinearly coupled, Newmark integration is employed to solve the system. The finite element equation can be discretized in the time domain as follows

$$[\mathbf{M}]\{\ddot{\mathbf{Q}}_{t+\Delta t}\} + [\mathbf{C}]\{\dot{\mathbf{Q}}_{t+\Delta t}\} + [\mathbf{K}]\{\mathbf{Q}_{t+\Delta t}\} = \{\mathbf{F}_{t+\Delta t}\}, \qquad (20)$$

where Δt represents the time increment. The generalized displacement $\{\mathbf{Q}\}$ is calculated from the following equation

$$\{\mathbf{Q}_{t+\Delta t}\} = [\hat{\mathbf{K}}]^{-1}\{\hat{\mathbf{F}}\}, \qquad (21)$$

where

$$[\hat{\mathbf{K}}] = [\mathbf{K}] + \alpha_0[\mathbf{M}] + \alpha_1[\mathbf{C}], \qquad (22)$$

$$\{\hat{\mathbf{F}}\} = \{\mathbf{F}_{t+\Delta t}\} + [\mathbf{M}](\alpha_0\{\mathbf{Q}_t\} + \alpha_2\{\dot{\mathbf{Q}}_t\} + \alpha_3\{\ddot{\mathbf{Q}}_t\}) + [\mathbf{C}](\alpha_1\{\mathbf{Q}_t\} + \alpha_4\{\dot{\mathbf{Q}}_t\} + \alpha_5\{\ddot{\mathbf{Q}}_t\}), \qquad (23)$$

where $[\mathbf{C}]$ is the damping matrix and $\alpha_{i,(i=0,1,...,7)}$ are the parameters of the Newmark solver. It can be seen from equations (21), (22), and (23) that the generalized displacement $\{\mathbf{Q}_{t+\Delta t}\}$ at the next time step is dependent on the excitation vector $\{\mathbf{F}_{t+\Delta t}\}$ at the next time step and the generalized displacement $\{\mathbf{Q}_t\}$, generalized velocity $\{\dot{\mathbf{Q}}_t\}$, and generalized acceleration $\{\ddot{\mathbf{Q}}_t\}$ at the current time step. Once the excitation vector at time step $t + \Delta t$ and initial conditions are known, the generalized displacement can be calculated from equation (21). Velocity and acceleration at the next time step can be approximated by

$$\{\ddot{\mathbf{Q}}_{t+\Delta t}\} = \alpha_0(\{\mathbf{Q}_{t+\Delta t}\} + \{\mathbf{Q}_t\}) - \alpha_2\{\dot{\mathbf{Q}}_t\} - \alpha_3\{\ddot{\mathbf{Q}}_t\},$$
$$\{\dot{\mathbf{Q}}_{t+\Delta t}\} = \{\dot{\mathbf{Q}}_t\} + \alpha_6\{\ddot{\mathbf{Q}}_t\} + \alpha_7\{\ddot{\mathbf{Q}}_{t+\Delta t}\}. \qquad (24)$$
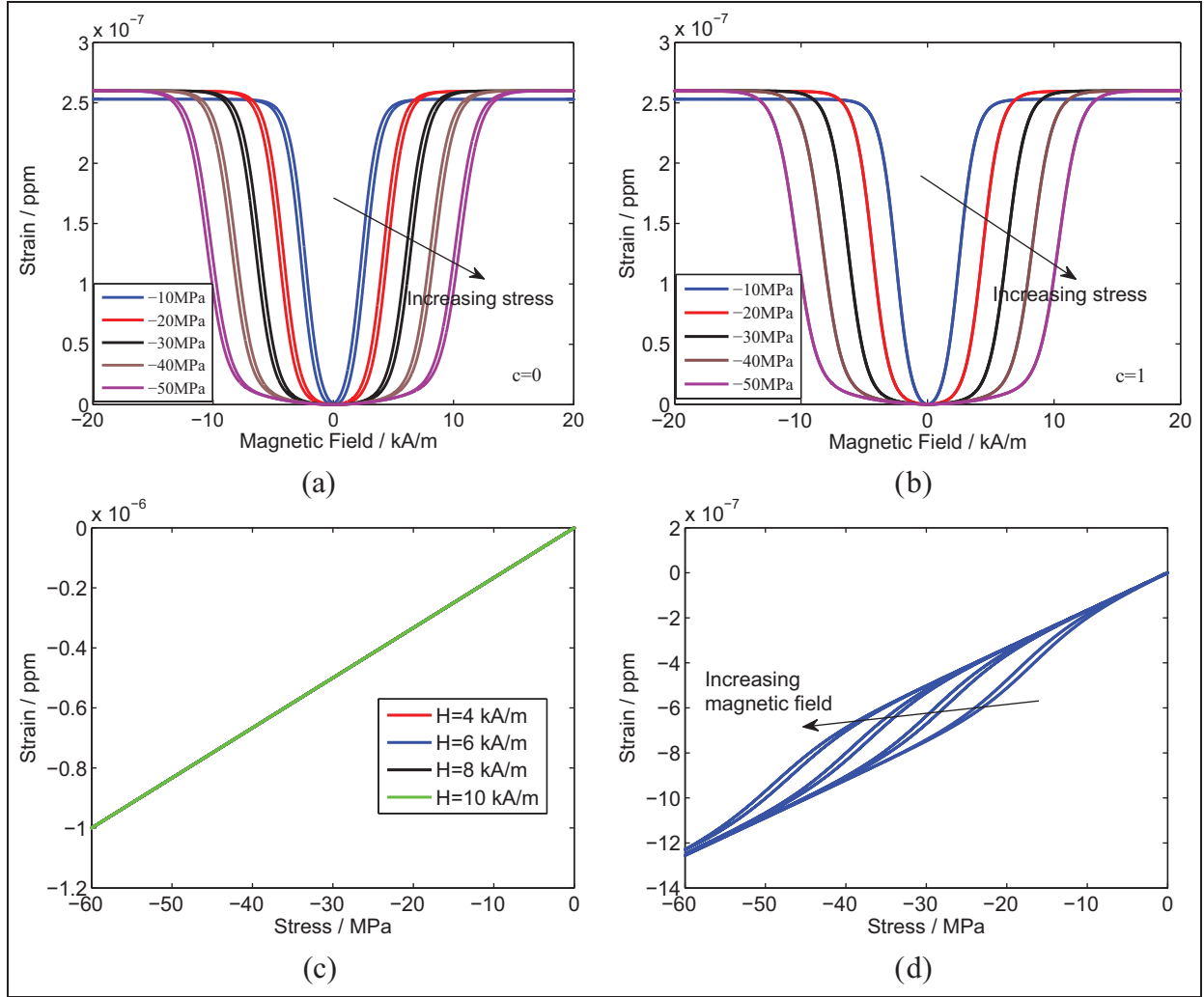
Figure 3. Simulation results of hysteresis model: (a) strain versus magnetic field at different constant stresses when $c = 0$, (b) strain versus magnetic field at different constant stresses when $c = 1$, (c) strain versus stress at different constant fields when volume fraction is calculated from equation (14) and (d) strain versus stress at different constant fields when volume fraction is calculated from equation (15).

The parameters in the Newmark integration are as follows

$$\alpha_0 = \frac{1}{\beta \Delta t^2}, \ \alpha_1 = \frac{\gamma}{\beta \Delta t}, \ \alpha_2 = \frac{1}{\beta \Delta t}, \ \alpha_3 = \frac{1}{2\beta} - 1,$$

$$\alpha_4 = \frac{\gamma}{\beta} - 1, \ \alpha_5 = \frac{\Delta t}{2}\left(\frac{\gamma}{\beta} - 2\right), \ \alpha_6 = \Delta t(1 - \gamma), \alpha_7 = \Delta t \gamma$$

$$(25)$$

where γ and β are the solver coefficients. In the proposed cantilever system, the left end is clamped such that the displacements and rotations are zero at that end. These boundary conditions can be applied using the elimination approach, namely, the entries in the matrices of equation (20) related to the clamped node can be eliminated. Furthermore, the excitation vector $[\mathbf{F}^{\lambda, u} \ \mathbf{F}^{\lambda, v}]^\top$ at time step $t + \Delta t$ contains the magnetostriction, which is a function of the strain and therefore

of displacement. As a result, the excitation vector is nonlinearly coupled with the generalized displacement $\{\mathbf{Q}_{t + \Delta t}\}$. This must be solved using an initial guess and iteration. From equation (19), it can be observed that the unidirectional magnetostriction λ is the sum of the magnetostrictions $\lambda^i(\mathbf{m}^i)$ due to each orientation, weighted by the volume fractions ζ^i. Hysteresis is included through the evolution of volume fractions (15). In order to calculate the evolution, we start the initial guess at increments of displacement $\{d\mathbf{Q}_{t + \Delta t}\}$, rather than $\{\mathbf{Q}_{t + \Delta t}\}$. The initial conditions are assumed to be zero. The procedure for approximating the nonlinear system is detailed in Table 1.

Verification of the solver

In order to verify the numerical solution from equations (21) and (24), the numerical solution from the

Table 1. Steps for approximating the nonlinear system.

(a)	Give an initial guess of $\{d\mathbf{Q}_{t+\Delta t}\}$.
(b)	Calculate the increments of strain $d\varepsilon_{t+\Delta t}$, magnetostriction $d\lambda$, and stress $d\sigma$.
(c)	Calculate the magnetostriction $\lambda_{t+\Delta t} = \lambda_t + d\lambda$ and the excitation vector $\left[\mathbf{F}_{t+\Delta t}^{\lambda,u}, \mathbf{F}_{t+\Delta t}^{\lambda,v}\right]^{\top}$.
(d)	Calculate the displacement $\{\mathbf{Q}_{t+\Delta t}\}$ using equation (21) and the velocity and acceleration using equation (24).
(e)	Compute the difference between the kth and $(k+1)$th iteration, $\Delta\hbar = \left\|\mathbf{Q}_{t+\Delta t}^{k+1} - \mathbf{Q}_{t+\Delta t}^{k}\right\|$; repeat the above steps until the condition $\Delta\hbar = \left\|\mathbf{Q}_{t+\Delta t}^{k+1} - \mathbf{Q}_{t+\Delta t}^{k}\right\| < \delta$ is satisfied.
(f)	Calculate the volume fraction $\zeta_{t+\Delta t} = \zeta_t + d\zeta$ and stress $\sigma_{g,t+\Delta t} = \sigma_{g,t} + d\sigma_g$, which are needed for the next time step.

Newmark solver is compared with the analytical solution obtained using beam theory. Both free vibration and harmonic responses are investigated.

Free vibration. The governing equation for a passive beam subjected to a load density $f(t,x)$ can be expressed as

$$EI\frac{\partial^4 w(t,x)}{\partial x^4} + \hat{c}\frac{\partial w(t,x)}{\partial t} + \rho A\frac{\partial^2 w(t,x)}{\partial t^2} = f(t,x) \quad (26)$$

where $\hat{c}$ is Kelvin–Voigt damping. For the case of free vibration, there is no external excitation applied to the beam. As detailed in Appendix 3, if the initial vertical displacement is $y_0(x)$ and the initial velocity is zero, then the analytical solution of equation (26) is given as

$$
\begin{aligned}
y(t,x) &= \sum_{n=1}^{\infty} W_n(x)q_n(t) \\
&= \sum_{n=1}^{\infty} W_n(x)\frac{\omega_n}{\omega_{dn}}\frac{1}{\int_0^L \rho A W_n^2(x)dx} \\
&\quad \times \int_0^L \rho A W_n(x)y_0(x)dx e^{-\zeta_n\omega_n t}\cos(\omega_{dn}t - \psi),
\end{aligned}
\quad (27)
$$

where $\psi = \tan^{-1}(\zeta_n\omega_n/\omega_{dn})$ and $W_n(x)$ denotes the nth order mode shape. In order to compare the results of the Newmark solver with the analytical solution (27), the finite element model of the passive beam, subjected to the same initial conditions, is rewritten as

$$
\begin{bmatrix} \mathbf{m}_e^u & 0 \\ 0 & \mathbf{m}_e^v \end{bmatrix}\begin{bmatrix} \ddot{\mathbf{q}}_e^u \\ \ddot{\mathbf{q}}_e^v \end{bmatrix} + \begin{bmatrix} \mathbf{c}_e^u & 0 \\ 0 & \mathbf{c}_e^v \end{bmatrix}\begin{bmatrix} \dot{\mathbf{q}}_e^u \\ \dot{\mathbf{q}}_e^v \end{bmatrix}
$$
$$
+ \begin{bmatrix} \mathbf{k}_e^u & -(\mathbf{k}^{uv})^{\top} \\ -(\mathbf{k}^{uv}) & \mathbf{k}_e^v \end{bmatrix}\begin{bmatrix} \mathbf{q}_e^u \\ \mathbf{q}_e^v \end{bmatrix} = \begin{bmatrix} \mathbf{0}_{(N_q^u \times 1)} \\ \mathbf{0}_{(N_q^v \times 1)} \end{bmatrix}.
\quad (28)
$$

The dynamic response of equation (28) only depends on the initial conditions of the generalized displacements $[\mathbf{q}_e^u \ \mathbf{q}_e^v]^{\top}$. Assuming that the initial deformation is caused by a concentrated load F_0 applied at the free end of the beam, the vertical displacement can be expressed as

$$v(x) = \frac{F_0 x^2}{6EI}(3L - x). \quad (29)$$

The exact expression for the curvature of the beam is

$$
\begin{aligned}
\kappa = \frac{1}{\tilde{\rho}} &= \frac{\frac{d^2 v(x)}{dx^2}}{\left[1 + \left(\frac{dv(x)}{dx}\right)^2\right]^{3/2}} \\
&= \frac{8E^2 I^2 F_0(L-x)}{\left(4F_0^2 L^2 x^2 - 4F_0^2 L x^3 + F_0^2 x^4 + 4E^2 I^2\right)^{3/2}}.
\end{aligned}
\quad (30)
$$

The horizontal displacement can be obtained by integrating the axial strain ε_x along the x-axis. If $\tilde{z}$ is the distance between the midplane and neutral plane, then the axial strain of the midplane is $\varepsilon_x = \kappa\tilde{z}$. Hence, the horizontal displacement can be calculated as

$$
\begin{aligned}
u(x) &= -\int_0^x \kappa(\tau)\tilde{z}d\tau \\
&= -\int_0^x \frac{8E^2 I^2 F_0(L-\tau)}{\left(4F_0^2 L^2 \tau^2 - 4F_0^2 L\tau^3 + F_0^2 \tau^4 + 4E^2 I^2\right)^{3/2}}\tilde{z}d\tau,
\end{aligned}
\quad (31)
$$

in which the position of the neutral plane needs to be known. This neutral plane position can be determined from a force balance equation

$$
\begin{aligned}
F &= \int_{A_s} \sigma_s dA_s + \int_{A_g} \sigma_g dA_g \\
&= -E_s \int_{h-t_g-t_s}^{h-t_g}\int_0^b (\kappa z)dydz - E_g \int_{h-t_g}^{h}\int_0^b (\kappa z)dydz \\
&= -\frac{1}{2}E_s\kappa b\left(2t_s(h-t_g) - t_s^2\right) - \frac{1}{2}E_g\kappa b\left(2ht_g - t_g^2\right) \\
&= 0,
\end{aligned}
\quad (32)
$$

where h denotes the distance from the top of the beam to the neutral line. Solving equation (32) for h gives

$$h = \frac{\frac{1}{2}\left(E_s t_s^2 + E_g t_g^2\right) + E_s t_s t_g}{E_s t_s + E_g t_g}. \quad (33)$$
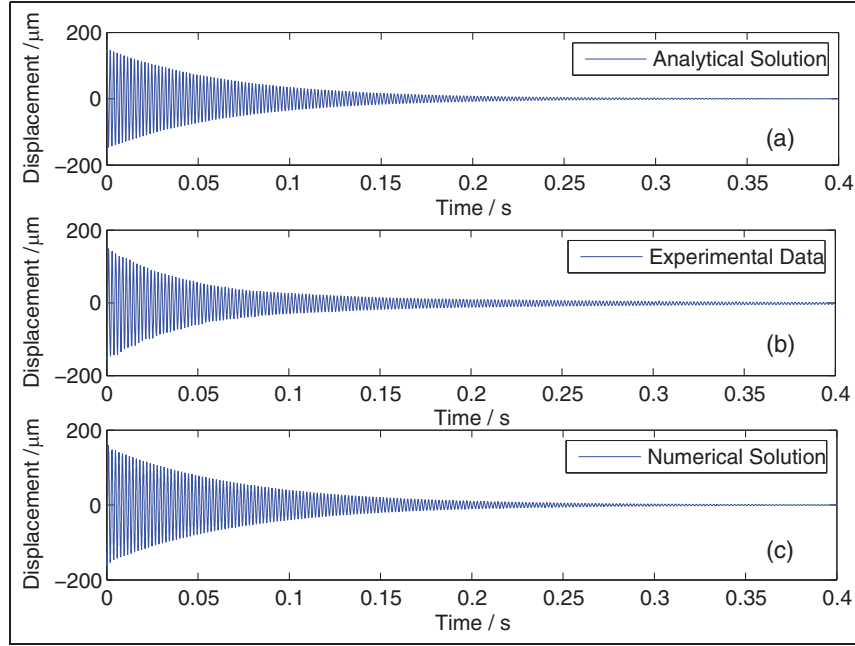
The initial horizontal displacement is therefore calculated as

Figure 4. Free vibration of the passive beam: (a) analytic solution, (b) experimental data, and (c) numerical solution.

$$u_0(x) = -\int_0^x \kappa(\tau)\left(h - \frac{t_g + t_s}{2}\right)d\tau$$

$$= -\int_0^x \frac{8E^2I^2F_0(L-\tau)}{\left(4F_0^2L^2\tau^2 - 4F_0^2L\tau^3 + F_0^2\tau^4 + 4E^2I^2\right)^{3/2}}$$

$$\left(\frac{\frac{1}{2}\left(E_st_s^2 + E_gt_g^2\right) + E_st_st_g}{E_st_s + E_gt_g} - \frac{t_s + t_g}{2}\right)d\tau. \tag{34}$$

In order to verify the numerical solver, the numerical solution calculated using equations (20) to (25) with initial deformation (34) needs to be compared with the analytical solution (27). Simulation results using analytical and numerical methods are illustrated in Figure 4(a) and (c), respectively. It can be seen that the numerical solution is consistent with the analytical solution. The Fast Fourier Transform of the decaying oscillations in Figure 4(a) and (c) is presented in Figure 5. Both solutions predict the same fundamental frequency. An experimental test (Figures 4(b) and 5) was conducted to verify the solutions. It is observed that the numerical and analytical solutions for displacement are consistent with the experimental data and that the finite element model (28) correctly predicts the system's fundamental frequency.

Forced vibration. We assume that a harmonic point force $F_d(t) = F_0\sin(\omega_i t)$ is applied at the free end of the cantilever and that the initial conditions for the vertical displacement and velocity are zero. As detailed in Appendix 3, the governing equation (26) can be
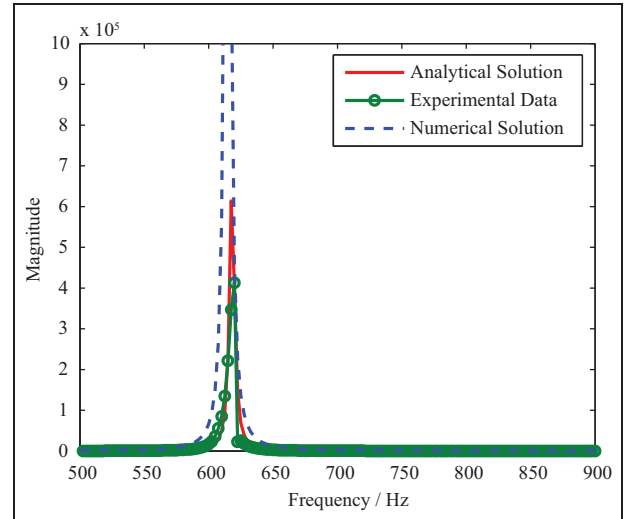

Figure 5. Fast Fourier Transform (FFT) of the decay (analytical solution, experimental data, and numerical solution).

analytically solved for the forced dynamic response in terms of vertical displacement as

$$y(t,x) = \sum_{n=1}^{\infty} W_n(x)q_n(t)$$

$$= \sum_{n=1}^{\infty} W_n(x)\frac{F_0W_n(L)}{\rho A \int_0^L W_n^2(x)dx}\frac{1}{\omega_{dn}} \tag{35}$$

$$\int_0^t \sin(\omega_i(t-\tau))e^{-\zeta_n\omega_n\tau}\sin\omega_{dn}\tau d\tau.$$
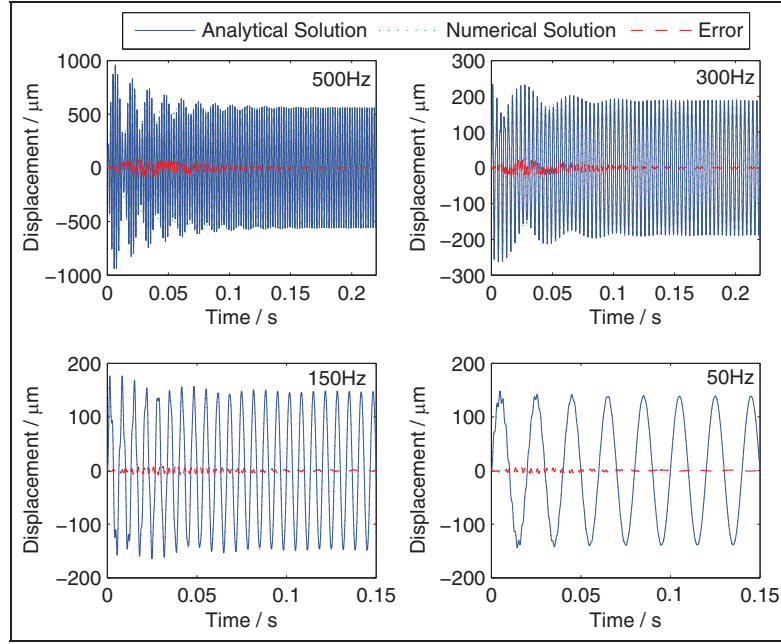
Figure 6. Analytical and numerical solutions for forced vibration of the passive beam.
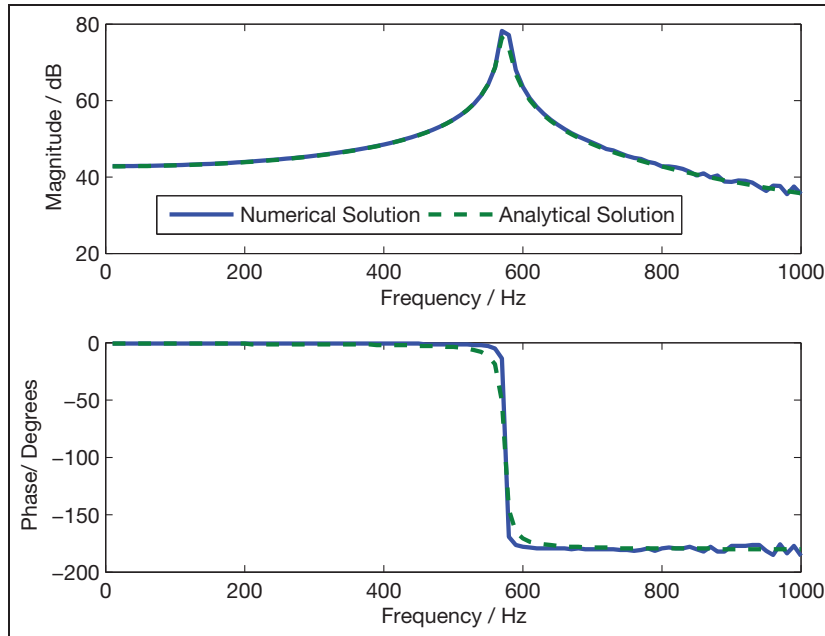

Figure 7. Frequency response of analytical and numerical solutions for forced vibration of the passive beam.

The finite element model for the passive beam, subjected to the same initial conditions and harmonic excitation, can be written as follows

$$
\begin{bmatrix} \mathbf{m}_e^u & 0 \\ 0 & \mathbf{m}_e^v \end{bmatrix} \begin{bmatrix} \ddot{\mathbf{q}}_e^u \\ \ddot{\mathbf{q}}_e^v \end{bmatrix} + \begin{bmatrix} \mathbf{c}_e^u & 0 \\ 0 & \mathbf{c}_e^v \end{bmatrix} \begin{bmatrix} \dot{\mathbf{q}}_e^u \\ \dot{\mathbf{q}}_e^v \end{bmatrix}
$$

$$
+ \begin{bmatrix} \mathbf{k}_e^u & -(\mathbf{k}^{uv})^\top \\ -(\mathbf{k}^{uv}) & \mathbf{k}_e^v \end{bmatrix} \begin{bmatrix} \mathbf{q}_e^u \\ \mathbf{q}_e^v \end{bmatrix} = \begin{bmatrix} \mathbf{0}_{N_q^u \times 1} \\ \mathbf{0}_{(N_q^v - 2) \times 1} \\ F_{d\,1 \times 1} \\ 0_{1 \times 1} \end{bmatrix}, \qquad (36)
$$

in which the concentrated vertical load is only applied to the end node. The loads on the other two DOFs of the node are zeros. Figure 6 compares (in the time domain) the prediction from the numerical solver with the analytical solution (35) at different frequencies ranging from 50 to 500 Hz. Figure 7 compares the frequency response of the prediction from the numerical solver with the analytical solution (35) at different frequencies ranging from 10 to 1000 Hz. The plot shows that the numerical calculations are consistent with the analytical solution in both magnitude and phase
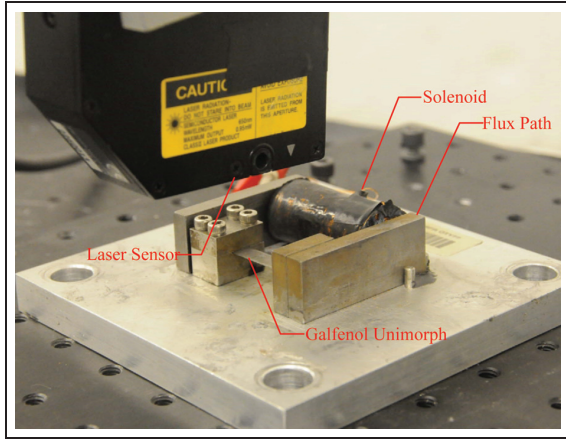
Figure 8. Experimental setup used for model validation and analysis.

responses. Calculation errors at the high frequencies are larger than the errors at low frequencies due to the limitation of the sampling frequency used in the numerical calculation. Higher sampling frequencies are needed at higher excitation frequencies to achieve the same calculation error.

Experimental results and discussion

Static and dynamic experiments were conducted in order to validate the nonlinear model. The applied magnetic field was assumed to be uniform along the length of the cantilever and throughout its thickness. Accordingly, a linear model was used for the field–current relationship, $H = NI$, with $N = 3300$ turns in the solenoid coil. The experimental setup, shown in Figure 8, used a laser sensor to measure tip displacement of the Galfenol unimorph and dSPACE ControlDesk for real-time manipulation. A sampling frequency of 10 kHz was used for the dSPACE system. Geometric and elastic parameters for both the Galfenol and substrate layers are shown in Table 2, and
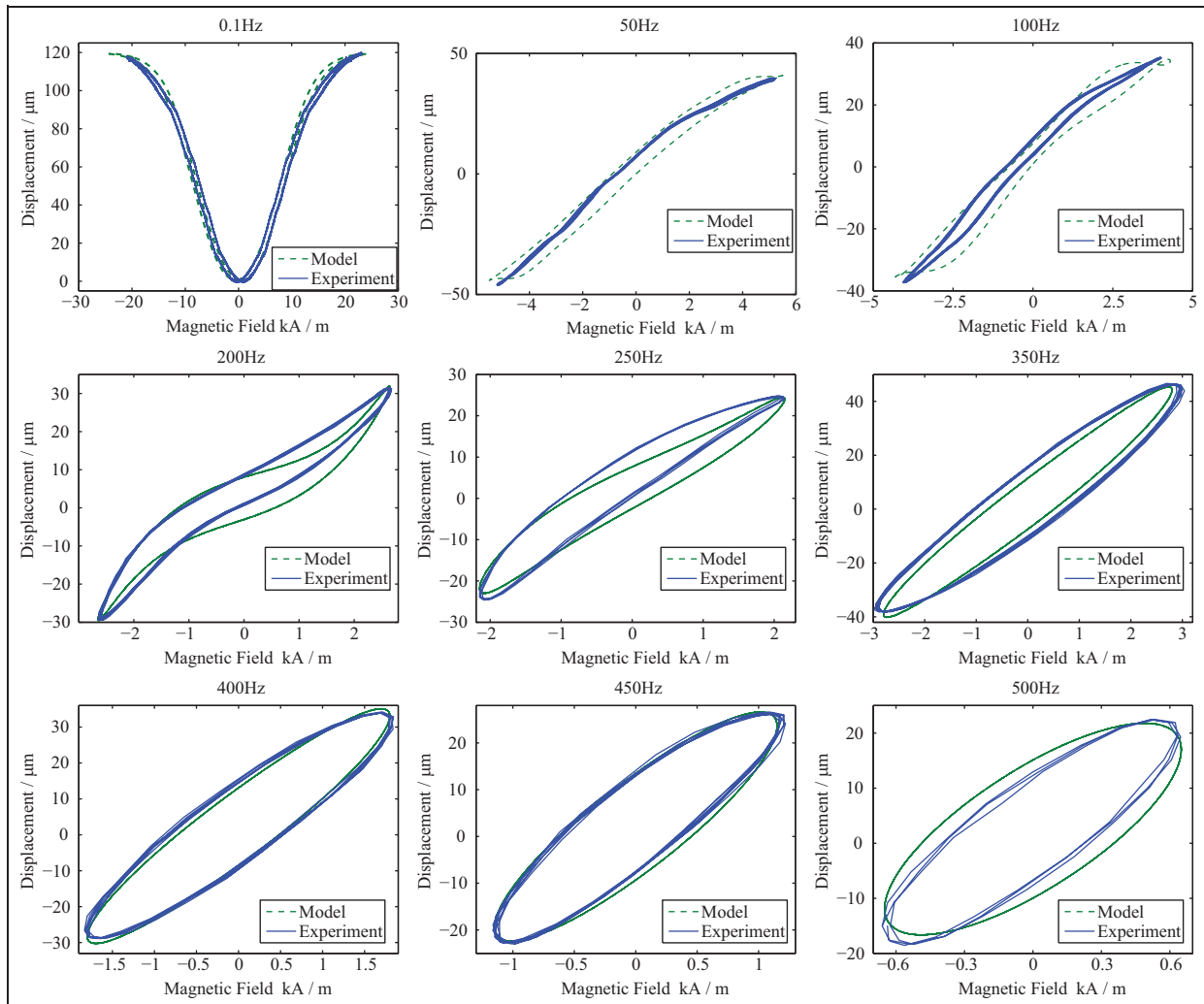

Figure 9. Comparison of nonlinear model calculations with static and dynamic experimental data for frequencies from 0.1 to 500 Hz.

Table 2. Geometric parameters for the composite layers.

Layers	L (mm)	b (mm)	t (mm)	E (GPa)	ρ (kg/m^3)
Galfenol	25	6.35	0.381	60	7870
Substrate	25	6.35	0.381	100	8400

Table 3. Material parameters for the Galfenol layer.

K_{100} (kJ/m^3)	30×10^3	$\mu_0 M_S$ (T)	1.6
λ_{100} (ppm)	$2/3 \times 280$	λ_{111} (ppm)	$1/3 \times (-20)$
Ω_s (kJ/m^3)	1200	c	0.1
E_p (kJ/m^3)	400		

the material parameters used to model the Galfenol constitutive behavior are shown in Table 3.

Figure 9 compares the finite element beam model with quasistatic and dynamic experimental results. In the quasistatic case, no bias magnetic field is applied and a full hysteresis loop is attained, demonstrating butterfly-type nonlinearity. Since deflection is an even function of the input field, no negative tip displacement is observed. In the dynamic case, a direct current (DC) bias current is applied and a sign change is observed in the deflection. The model accurately describes the changing shape of the hysteresis loop and peak-to-peak deflection with increasing frequency. While the hysteretic behavior of the material constitutive model is frequency independent, it can be seen that the hysteresis loop becomes wider as the frequency increases. This additional lag at high frequencies, which results mainly from the system vibrations and dynamic magnetic losses, is accurately described by the dynamic nonlinear model.

Concluding remarks

Galfenol's steel-like structural properties motivate its application in laminated devices. A fully coupled magnetoelastic model was developed to describe the nonlinear dynamic response of a Galfenol unimorph actuator. The hysteretic behavior of Galfenol was modeled by a discrete energy-averaged model, and the structural dynamics were incorporated using a finite element model. The magnetic hysteresis model was found to describe magnetic hysteresis for both field and stress inputs. A numerical solver was developed to calculate the nonlinear coupling between the magnetostriction and output displacements. The solver was verified for a passive beam, with the numerical solution shown to be consistent with both the analytical solution using beam theory and with the experimental data. Finally, the nonlinear magnetoelastic model was experimentally verified with the beam actuator excited between 0.1 and 500 Hz. Both the experimental data and model results show that the hysteresis loop becomes wider as the frequency increases. This dynamic nonlinearly coupled model accurately describes the frequency-dependent hysteresis loop shape and the peak-to-peak deflections, without the need for adjustable parameters.

References

Armstrong WD (2003) An incremental theory of magnetoelastic hysteresis in pseudo-cubic ferro-magnetostrictive alloys. *Journal of Magnetism and Magnetic Materials* 263(1–2): 208–218.

Atulasimha J, Akhras G and Flatau AB (2008) Comprehensive three dimensional hysteretic magnetomechanical model and its validation with experimental 110 single-crystal iron-gallium behavior. *Journal of Applied Physics* 103(7): 07B336.

Baillargeon BP and Vel SS (2005) Active vibration suppression of sandwich beams using piezoelectric shear actuators: experiments and numerical simulations. *Journal of Intelligent Material Systems and Structures* 16(6): 517–530.

Basantkumar RR, Stadler BJ, Robbins WP, et al. (2006) Integration of thin-film Galfenol with MEMS cantilevers for magnetic actuation. *IEEE Transactions on Magnetics* 42(10): 3102–3104.

Datta S, Atulasimha J, Mudivarthi C, et al. (2008) The modeling of magnetomechanical sensors in laminated structures. *Smart Materials and Structures* 17(2): 025010.

Datta S, Atulasimha J, Mudivarthi C, et al. (2009) Modeling of magnetomechanical actuators in laminated structures. *Journal of Intelligent Material Systems and Structures* 20(9): 1121–1135.

Downey PR and Flatau AB (2005) Magnetoelastic bending of Galfenol for sensor applications. *Journal of Applied Physics* 97(10): 10R505.

Du Tremolet de Lacheisserie E and Peuzin JC (1994) Magnetostriction and internal stresses in thin films: the cantilever method revisited. *Journal of Magnetism and Magnetic Materials* 136(1–2): 189–196.

Evans PG and Dapino MJ (2008) State-space constitutive model for magnetization and magnetostriction of Galfenol alloys. *IEEE Transactions on Magnetics* 44(7): 1711–1720.

Evans PG and Dapino MJ (2010) Efficient magnetic hysteresis model for field and stress application in magnetostrictive Galfenol. *Journal of Applied Physics* 107(6): 063906.

Gehring GA, Cooke MD, Gregory IS, et al. (2000) Cantilever unified theory and optimization for sensors and actuators. *Smart Materials and Structures* 9(6): 918–931.

Guerrero VH and Wetherhold RC (2003) Magnetostrictive bending of cantilever beams and plates. *Journal of Applied Physics* 94(10): 6659–6666.

Jia ZY, Liu W, Zhang YS, et al. (2006) A nonlinear magneto-mechanical coupling model of giant magnetostrictive thin films at low magnetic fields. *Sensors and Actuators A: Physical* 128(1): 158–164.

Jiles DC and Atherton DL (1986) Theory of ferromagnetic hysteresis. *Journal of Magnetism and Magnetic Materials* 61(1–2): 48–60.

Mudivarthi C, Datta S, Atulasimha J, et al. (2008) A bidirectionally coupled magnetoelastic model and its validation using a Galfenol unimorph sensor. *Smart Materials and Structures* 17(3): 035005.

Quandt E and Ludwig A (2000) Magnetostrictive actuation in microsystems. *Sensors and Actuators A: Physical* 81(1): 275–280.

Shu L, Dapino MJ, Evans PJ, et al. (2010) Optimization and dynamic modeling of Galfenol unimorphs. *Journal of Intelligent Material Systems and Structures* 22(8): 781–793.

Smith RC (1998) A nonlinear optimal control method for magnetostrictive actuators. *Journal of Intelligent Material Systems and Structures* 9(6): 468–485.

Stoner EC and Wohlfarth EP (1948) A mechanism of magnetic hysteresis in heterogeneous alloys. *Philosophical Transactions of the Royal Society A: Mathematical Physical and Engineering Sciences* 240: 599–642.

Ueno T and Higuchi T (2008) Two-DOF micro magnetostrictive bending actuator for wobbling motion. *IEEE Transactions on Magnetics* 44(11): 4078–4080.

Wang YZ, Atulasimha J, Clarke J, et al. (2010) Thickness ratio effects on quasistatic actuation and sensing behavior of laminate magnetoelectric cantilevers. *Proceedings of SPIE: The International Society for Optical Engineering* 764414.

Zhou HM and Zhou YH (2007) Vibration suppression of laminated composite beams using actuators of giant magnetostrictive materials. *Smart Materials and Structures* 16(1): 198–206.

Appendix 1

Derivation of internal virtual work

The internal virtual work due to stress is

$$
\begin{aligned}
\delta W_\sigma &= \int\limits_0^L \int\limits_A \sigma \delta \varepsilon \, dA \, dx \\
&= \int\limits_0^L \int\limits_{A_g} \sigma_g \delta \varepsilon_g \, dA_g \, dx + \int\limits_0^L \int\limits_{A_s} \sigma_s \delta \varepsilon_s \, dA_s \, dx \\
&= -\int\limits_0^L \int\limits_{A_g} E_g \left(\frac{\partial^2 v(t,x)}{\partial x^2} z + \lambda - \frac{\partial u(t,x)}{\partial x} \right) \delta \left(\frac{\partial u(t,x)}{\partial x} - \frac{\partial^2 v(t,x)}{\partial x^2} z \right) dA_g \, dx \\
&\quad - \int\limits_0^L \int\limits_{A_s} E_s \left(\frac{\partial^2 v(t,x)}{\partial x^2} z - \frac{\partial u(t,x)}{\partial x} \right) \delta \left(\frac{\partial u(t,x)}{\partial x} - \frac{\partial^2 v(t,x)}{\partial x^2} z \right) dA_s \, dx.
\end{aligned}
$$
(37)

Substituting equation (2) and expanding equation (37) gives the following

$$
\begin{aligned}
\delta W_\sigma &= E_g \int\limits_0^L \int\limits_{A_g} \frac{\partial^2 v(t,x)}{\partial x^2} z \delta \frac{\partial^2 v(t,x)}{\partial x^2} z \, dA_g \, dx \\
&\quad - E_g \int\limits_0^L \int\limits_{A_g} \frac{\partial^2 v(t,x)}{\partial x^2} z \delta \frac{\partial u(t,x)}{\partial x} \, dA_g \, dx \\
&\quad - E_g \int\limits_0^L \int\limits_{A_g} \frac{\partial u(t,x)}{\partial x} \delta \frac{\partial^2 v(t,x)}{\partial x^2} z \, dA_g \, dx \\
&\quad + E_g \int\limits_0^L \int\limits_{A_g} \frac{\partial u(t,x)}{\partial x} \delta \frac{\partial u(t,x)}{\partial x} \, dA_g \, dx \\
&\quad + E_g \int\limits_0^L \int\limits_{A_g} \lambda \delta \frac{\partial^2 v(t,x)}{\partial x^2} z \, dA_g \, dx \\
&\quad - E_g \int\limits_0^L \int\limits_{A_g} \lambda \delta \frac{\partial u(t,x)}{\partial x} \, dA_g \, dx \\
&\quad + E_s \int\limits_0^L \int\limits_{A_s} \frac{\partial^2 v(t,x)}{\partial x^2} z \delta \frac{\partial^2 v(t,x)}{\partial x^2} z \, dA_s \, dx \\
&\quad - E_s \int\limits_0^L \int\limits_{A_s} \frac{\partial^2 v(t,x)}{\partial x^2} z \delta \frac{\partial u(t,x)}{\partial x} \, dA_s \, dx \\
&\quad - E_s \int\limits_0^L \int\limits_{A_s} \frac{\partial u(t,x)}{\partial x} \delta \frac{\partial^2 v(t,x)}{\partial x^2} z \, dA_s \, dx \\
&\quad + E_s \int\limits_0^L \int\limits_{A_s} \frac{\partial u(t,x)}{\partial x} \delta \frac{\partial u(t,x)}{\partial x} \, dA_s \, dx.
\end{aligned}
$$
(38)

Collecting z in equation (38) gives

$$
\begin{aligned}
\delta W_\sigma &= E_g \int\limits_0^L \frac{\partial^2 v(t,x)}{\partial x^2} \delta \frac{\partial^2 v(t,x)}{\partial x^2} \left(\int\limits_{A_g} z^2 \, dA_g \right) dx \\
&\quad - E_g \int\limits_0^L \frac{\partial^2 v(t,x)}{\partial x^2} \delta \frac{\partial u(t,x)}{\partial x} \left(\int\limits_{A_g} z \, dA_g \right) dx \\
&\quad - E_g \int\limits_0^L \frac{\partial u(t,x)}{\partial x} \delta \frac{\partial^2 v(t,x)}{\partial x^2} \left(\int\limits_{A_g} z \, dA_g \right) dx \\
&\quad + E_g \int\limits_0^L \frac{\partial u(t,x)}{\partial x} \delta \frac{\partial u(t,x)}{\partial x} \left(\int\limits_{A_g} dA_g \right) dx
\end{aligned}
$$

$$+ E_g \int_0^L \int_{A_g} \lambda \delta \frac{\partial^2 v(t,x)}{\partial x^2} z \, dA_g \, dx$$

$$- E_g \int_0^L \int_{A_g} \lambda \delta \frac{\partial u(t,x)}{\partial x} \, dA_g \, dx$$

$$+ E_s \int_0^L \frac{\partial^2 v(t,x)}{\partial x^2} \delta \frac{\partial^2 v(t,x)}{\partial x^2} \left(\int_{A_s} z^2 \, dA_s \right) dx$$

$$- E_s \int_0^L \frac{\partial^2 v(t,x)}{\partial x^2} \delta \frac{\partial u(t,x)}{\partial x} \left(\int_{A_s} z \, dA_s \right) dx \qquad (39)$$

$$- E_s \int_0^L \frac{\partial u(t,x)}{\partial x} \delta \frac{\partial^2 v(t,x)}{\partial x^2} \left(\int_{A_s} z \, dA_s \right) dx$$

$$+ E_s \int_0^L \frac{\partial u(t,x)}{\partial x} \delta \frac{\partial u(t,x)}{\partial x} \left(\int_{A_s} dA_s \right) dx.$$

The cross section of the cantilever is assumed to be uniform. Integrating equation (39) along the y and z directions, the internal virtual work due to stress can be written as

$$\delta W_\sigma = E_g I_g \int_0^L \frac{\partial^2 v(t,x)}{\partial x^2} \delta \frac{\partial^2 v(t,x)}{\partial x^2} \, dx$$

$$- E_g Q_g \int_0^L \frac{\partial^2 v(t,x)}{\partial x^2} \delta \frac{\partial u(t,x)}{\partial x} \, dx - E_g Q_g \int_0^L \frac{\partial u(t,x)}{\partial x} \delta \frac{\partial^2 v(t,x)}{\partial x^2} \, dx$$

$$+ E_g A_g \int_0^L \frac{\partial u(t,x)}{\partial x} \delta \frac{\partial u(t,x)}{\partial x} \, dx + E_g \int_0^L \int_{A_g} \lambda \delta \frac{\partial^2 v(t,x)}{\partial x^2} z \, dA_g \, dx$$

$$- E_g \int_0^L \int_{A_g} \lambda \delta \frac{\partial u(t,x)}{\partial x} \, dA_g \, dx + E_s I_s \int_0^L \frac{\partial^2 v(t,x)}{\partial x^2} \delta \frac{\partial^2 v(t,x)}{\partial x^2} \, dx$$

$$- E_s Q_s \int_0^L \frac{\partial^2 v(t,x)}{\partial x^2} \delta \frac{\partial u(t,x)}{\partial x} \, dx - E_s Q_s \int_0^L \frac{\partial u(t,x)}{\partial x} \delta \frac{\partial^2 v(t,x)}{\partial x^2} \, dx$$

$$+ E_s A_s \int_0^L \frac{\partial u(t,x)}{\partial x} \delta \frac{\partial u(t,x)}{\partial x} \, dx, \qquad (40)$$

where

$$I_g = \int_{A_g} z^2 \, dA_g, \quad Q_g = \int_{A_g} z \, dA_g$$

$$I_s = \int_{A_s} z^2 \, dA_s, \quad Q_s = \int_{A_s} z \, dA_s.$$

Appendix 2

Discretization of weak form equation

The Hermite shape function vector is chosen as

$$H_1 = \frac{1}{4}(1-\xi)^2(2+\xi), \quad H_2 = \frac{1}{4}(1-\xi)^2(1+\xi)$$

$$H_3 = \frac{1}{4}(1+\xi)^2(2-\xi), \quad H_4 = \frac{1}{4}(1+\xi)^2(\xi-1). \qquad (41)$$

The linear shape function is chosen as

$$N_1 = \frac{1-\xi}{2}, \quad N_2 = \frac{1+\xi}{2}. \qquad (42)$$

Since the local spatial coordinate ξ varies from -1 to 1, the coordinate transformation is interpolated as

$$x = \frac{1-\xi}{2} x_1 + \frac{1+\xi}{2} x_2$$

$$= \frac{x_1 + x_2}{2} + \frac{x_2 - x_1}{2} \xi. \qquad (43)$$

Since $l_e = x_2 - x_1$ is the length of the element, we have

$$dx = \frac{l_e}{2} d\xi. \qquad (44)$$

Thus, the derivatives in equation (4) can be rewritten as

$$\frac{\partial^2 v(t,x)}{\partial x^2} = \frac{4}{l_e^2} \frac{\partial^2 v(t,x)}{\partial \xi^2} = \frac{4}{l_e^2} \frac{d^2 \mathbf{H}}{d\xi^2} \mathbf{q}_e^v$$

$$= \frac{4}{l_e^2} \left[\frac{3}{2}\xi, \frac{l_e}{4}(-1+3\xi), -\frac{3}{2}\xi, \frac{l_e}{4}(1+3\xi) \right] \mathbf{q}_e^v \qquad (45)$$

$$\frac{\partial u(t,x)}{\partial x} = \frac{2}{l_e} \frac{\partial u(t,x)}{\partial \xi} = \frac{2}{l_e} \left[-\frac{1}{2}, \frac{1}{2} \right] \mathbf{q}_e^u = \mathbf{B} \cdot \mathbf{q}_e^u.$$

Substituting equation (45) into equation (4), the virtual work due to stress can be written as

$$\delta W_\sigma = \sum_e EI \int_{-1}^{1} \frac{4}{l_e^2} \frac{d^2\mathbf{H}}{d\xi^2} \mathbf{q}_e^v \delta\left(\frac{4}{l_e^2} \frac{d^2\mathbf{H}}{d\xi^2} \mathbf{q}_e^v\right) \frac{l_e}{2} d\xi$$

$$- EQ \int_{-1}^{1} \frac{4}{l_e^2} \frac{d^2\mathbf{H}}{d\xi^2} \mathbf{q}_e^v \delta\left(\mathbf{B} \cdot \mathbf{q}_e^u\right) \frac{l_e}{2} d\xi$$

$$- EQ \int_{-1}^{1} \mathbf{B} \cdot \mathbf{q}_e^u \delta\left(\frac{4}{l_e^2} \frac{d^2\mathbf{H}}{d\xi^2} \mathbf{q}_e^v\right) \frac{l_e}{2} d\xi$$

$$+ EA \int_{-1}^{1} \mathbf{B} \cdot \mathbf{q}_e^u \delta\left(\mathbf{B} \cdot \mathbf{q}_e^u\right) \frac{l_e}{2} d\xi$$

$$+ E_g \int_{-1}^{1} \int_{A_g} \lambda(H, q, \sigma) z \delta\left(\frac{4}{l_e^2} \frac{d^2\mathbf{H}}{d\xi^2} \mathbf{q}_e^v\right) \frac{l_e}{2} dA_g d\xi$$

$$- E_g \int_{-1}^{1} \int_{A_g} \lambda(H, q, \sigma) \delta\left(\mathbf{B} \cdot \mathbf{q}_e^u\right) \frac{l_e}{2} dA_g d\xi$$

$$= \sum_e \mathbf{q}_e^{v\top} \cdot \left[\frac{8EI}{l_e^3} \int_{-1}^{1} \left(\frac{d^2\mathbf{H}}{d\xi^2}\right)^\top \frac{d^2\mathbf{H}}{d\xi^2} d\xi\right] \delta\mathbf{q}_e^v$$

$$- \mathbf{q}_e^{v\top} \cdot \left[\frac{2EQ}{l_e} \int_{-1}^{1} \left(\frac{d^2\mathbf{H}}{d\xi^2}\right)^\top \mathbf{B} d\xi\right] \delta\mathbf{q}_e^u$$

$$- \mathbf{q}_e^{u\top} \cdot \left[\frac{2EQ}{l_e} \int_{-1}^{1} \mathbf{B} \frac{d^2\mathbf{H}}{d\xi^2} d\xi\right] \delta\mathbf{q}_e^v + \mathbf{q}_e^{u\top} \cdot \left[EAl_e \mathbf{B}^\top \cdot \mathbf{B}\right] \delta\mathbf{q}_e^u$$

$$+ \left[\frac{2E_g b}{l_e} \int_{-1}^{1} \int_{t_g} \lambda(H, q, \sigma) z \frac{d^2\mathbf{H}}{d\xi^2} dz d\xi\right] \delta\mathbf{q}_e^v$$

$$- \left[\frac{E_g b l_e}{2} \int_{-1}^{1} \int_{t_g} \lambda(H, q, \sigma) \mathbf{B} dz d\xi\right] \delta\mathbf{q}_e^u$$

$$= \sum_e \mathbf{q}_e^{v\top} \cdot \mathbf{k}_e^v \delta\mathbf{q}_e^v - \mathbf{q}_e^{v\top} \cdot \mathbf{k}_e^{uv} \delta\mathbf{q}_e^u - \mathbf{q}_e^{u\top} \cdot \left(\mathbf{k}_e^{uv}\right)^\top \delta\mathbf{q}_e^v$$

$$+ \mathbf{q}_e^{u\top} \cdot \mathbf{k}_e^u \delta\mathbf{q}_e^u + \mathbf{f}_e^{\lambda, v} \delta\mathbf{q}_e^v - \mathbf{f}_e^{\lambda, u} \delta\mathbf{q}_e^u. \tag{46}$$

From (5), the virtual work components due to inertial and damping effects are

$$\delta W_\rho = \int_0^L \int_A \rho \frac{\partial^2 u(t,x)}{\partial t^2} \delta u dA dx + \int_0^L \int_A \rho \frac{\partial^2 v(t,x)}{\partial t^2} \delta v dA dx$$

$$\delta W_c = \int_0^L \int_A c \frac{\partial u(t,x)}{\partial t} \delta u dA dx + \int_0^L \int_A c \frac{\partial v(t,x)}{\partial t} \delta v dA dx. \tag{47}$$

Substitution of equation (7) and equation (8) into equation (47) gives

$$\delta W_\rho = \sum_e \int_{-1}^{1} \int_A \rho\left(\mathbf{N} \cdot \ddot{\mathbf{q}}_e^u\right)^\top \delta\left(\mathbf{N} \cdot \mathbf{q}_e^u\right) \frac{l_e}{2} dA d\xi$$

$$+ \int_{-1}^{1} \int_A \rho\left(\mathbf{H} \cdot \ddot{\mathbf{q}}_e^v\right)^\top \delta\left(\mathbf{H} \cdot \mathbf{q}_e^v\right) \frac{l_e}{2} dA d\xi$$

$$= \sum_e \ddot{\mathbf{q}}_e^{u\top} \cdot \left[\frac{l_e \rho A}{2} \int_{-1}^{1} \mathbf{N}^\top \cdot \mathbf{N} d\xi\right] \delta\mathbf{q}_e^u$$

$$+ \ddot{\mathbf{q}}_e^{v\top} \cdot \left[\frac{l_e \rho A}{2} \int_{-1}^{1} \mathbf{H}^\top \cdot \mathbf{H} d\xi\right] \delta\mathbf{q}_e^v$$

$$= \sum_e \left\{\ddot{\mathbf{q}}_e^u\right\}^\top \cdot \left[\mathbf{m}_e^u\right] \left\{\delta\mathbf{q}_e^u\right\} + \left\{\ddot{\mathbf{q}}_e^v\right\}^\top \cdot \left[\mathbf{m}_e^v\right] \left\{\delta\mathbf{q}_e^v\right\} \tag{48}$$

$$\delta W_c = \int_0^L \int_A c\dot{u}\delta u dA dx + \int_0^L \int_A c\dot{v}\delta v dA dx$$

$$= \sum_e \int_{-1}^{1} \int_A c\left(\mathbf{N} \cdot \dot{\mathbf{q}}_e^u\right)^\top \delta\left(\mathbf{N} \cdot \mathbf{q}_e^u\right) \frac{l_e}{2} dA d\xi$$

$$+ \int_{-1}^{1} \int_A c\left(\mathbf{H} \cdot \dot{\mathbf{q}}_e^v\right)^\top \delta\left(H \cdot q_e^v\right) \frac{l_e}{2} dA d\xi$$

$$= \sum_e \dot{\mathbf{q}}_e^{u\top} \cdot \left[\frac{l_e c A}{2} \int_{-1}^{1} \mathbf{N}^\top \cdot \mathbf{N} d\xi\right] \delta\mathbf{q}_e^u$$

$$+ \dot{\mathbf{q}}_e^{v\top} \cdot \left[\frac{l_e c A}{2} \int_{-1}^{1} \mathbf{H}^\top \cdot \mathbf{H} d\xi\right] \delta\mathbf{q}_e^v$$

$$= \sum_e \left\{\dot{\mathbf{q}}_e^u\right\}^\top \cdot \left[\mathbf{c}_e^u\right] \left\{\delta\mathbf{q}_e^u\right\} + \left\{\dot{\mathbf{q}}_e^v\right\}^\top \cdot \left[\mathbf{c}_e^v\right] \left\{\delta\mathbf{q}_e^v\right\}. \tag{49}$$

Setting the sum of the discretized virtual work due to the internal stress (46), inertia (48), and damping effects (49) equal to zero, the discretized weak form equation can be written as

$$\sum_e \left\{\mathbf{q}_e^v\right\}^\top \cdot \left[\mathbf{k}_e^v\right] \left\{\delta\mathbf{q}_e^v\right\} - \left\{\mathbf{q}_e^v\right\}^\top \cdot \left[\mathbf{k}_e^{uv}\right] \left\{\delta\mathbf{q}_e^u\right\}$$

$$- \left\{\mathbf{q}_e^u\right\}^\top \cdot \left[\mathbf{k}_e^{uv}\right]^\top \left\{\delta\mathbf{q}_e^v\right\} + \left\{\mathbf{q}_e^u\right\}^\top \cdot \left[\mathbf{k}_e^u\right] \left\{\delta\mathbf{q}_e^u\right\}$$

$$+ \sum_e \left\{\ddot{\mathbf{q}}_e^u\right\}^\top \cdot \left[\mathbf{m}_e^u\right] \left\{\delta\mathbf{q}_e^u\right\} + \left\{\ddot{\mathbf{q}}_e^v\right\}^\top \cdot \left[\mathbf{m}_e^v\right] \left\{\delta\mathbf{q}_e^v\right\}$$

$$+ \sum_e \left\{\dot{\mathbf{q}}_e^u\right\}^\top \cdot \left[\mathbf{c}_e^u\right] \left\{\delta\mathbf{q}_e^u\right\} + \left\{\dot{\mathbf{q}}_e^v\right\}^\top \cdot \left[\mathbf{c}_e^v\right] \left\{\delta\mathbf{q}_e^v\right\}$$

$$= \sum_e -\left[\mathbf{f}_e^{\lambda, v}\right] \left\{\delta\mathbf{q}_e^v\right\} + \left[\mathbf{f}_e^{\lambda, u}\right] \left\{\delta\mathbf{q}_e^u\right\}. \tag{50}$$

Appendix 3

Analytical solution of passive beam

The response of a passive beam is determined by first solving for the general solution. Then, solutions for the cases of free vibration and forced harmonic response are obtained by applying different loads and initial conditions to the general solution. The governing equation for a passive beam, subjected to load density $f(t, x)$, can be written as

$$EI\frac{\partial^4 w(t,x)}{\partial x^4} + \hat{c}\frac{\partial w(t,x)}{\partial t} + \rho A\frac{\partial^2 w(t,x)}{\partial t^2} = f(t,x) \quad (51)$$

where $\hat{c}$ is Kelvin–Voigt damping. Using modal analysis, the solution of equation (51) can be expressed as

$$w(t,x) = \sum_{n=1}^{\infty} W_n(x)q_n(t). \quad (52)$$

Here, $W_n(x)$ denotes the nth mode shape of the cantilever, which can be expressed as

$$W_n(x) = C_n[\sin\beta_n x - \sinh\beta_n x - \alpha_n(\cos\beta_n x - \cosh\beta_n x)] \quad (53)$$

where $\alpha_n = (\sin\beta_n l + \sinh\beta_n l)/(\cos\beta_n l + \cosh\beta_n l)$ and the frequency equation is $\cos\beta_n l \cdot \cosh\beta_n l = -1$. Substitution of equation (52) into equation (51) gives

$$EI\sum_{n=1}^{\infty}\frac{d^4 W_n(x)}{dx^4}q_n(t) + \rho A\sum_{n=1}^{\infty}W_n(x)\frac{d^2 q_n(t)}{dt^2} \\ + \hat{c}\sum_{n=1}^{\infty}W_n(x)\frac{dq_n(t)}{dt} = f(t,x). \quad (54)$$

Since

$$EI\frac{d^4 W_n(x)}{dx^4} = \omega_n^2 \rho A W_n(x), \quad (55)$$

(54) can be rewritten as

$$\sum_{n=1}^{\infty}\omega_n^2 \rho A W_n(x)q_n(t) + \rho A\sum_{n=1}^{\infty}W_n(x)\frac{d^2 q_n(t)}{dt^2} \\ + \hat{c}\sum_{n=1}^{\infty}W_n(x)\frac{dq_n(t)}{dt} = f(t,x). \quad (56)$$

By multiplying equation (56) throughout by $W_m(x)$, integrating from 0 to L, and using the orthogonality condition, we obtain

$$\frac{d^2 q_n(t)}{dt^2} + \frac{\hat{c}}{\rho A}\frac{dq_n(t)}{dt} + \omega_n^2 q_n(t) \\ = \frac{1}{\rho A\int_0^L W_n^2(x)dx}\int_0^L f(x,t)W_n(x)dx. \quad (57)$$

The problem investigated here is for a point load applied at the end of the passive beam. The integral in equation (57) can thus be simplified as

$$\int_0^L f(x,t)W_n(x)dx = \int_0^L W_n(x)F_0 u(t)\delta(x-L)dx = F_0 u(t)W_n(L) \quad (58)$$

where F_0 is the magnitude of the force, $\delta(\cdot)$ is the Dirac delta function, and $u(t)$ is the trajectory of the load in the time domain. Substituting equation (58) into equation (57) and solving analytically, one obtains the modal displacement

$$q_n(t) = \frac{1}{\rho A\int_0^L W_n^2(x)dx}\frac{1}{\omega_{dn}}F_0 W_n(L) \\ \int_0^t u(t-\tau)e^{-\zeta_n\omega_n\tau}\sin\omega_{dn}\tau d\tau + \frac{q_n(0)\omega_n}{\omega_{dn}} \\ e^{-\zeta_n\omega_n t}\cos(\omega_{dn}t - \psi) + \frac{\dot{q}_n(0)}{\omega_{dn}}e^{-\zeta_n\omega_n t}\sin\omega_{dn}t \quad (59)$$

where ω_n is the nth order natural frequency, ω_{dn} is the damped natural frequency, and $q_n(0)$ and $\dot{q}_n(0)$ are the initial modal displacement and velocity, respectively. To express the initial modal displacement in terms of the actual initial displacement function $y_0(x)$, we let $t = 0$ in equation (52) and write

$$y(0,x) = \sum_{n=1}^{\infty}W_n(x)q_n(0) = y_0(x). \quad (60)$$

Then, multiplying equation (60) by $\rho A W_n(x)$, integrating over the length of the beam, and using the orthonormality relations, we obtain

$$q_n(0) = \frac{1}{\int_0^L \rho A W_n^2(x)dx}\int_0^L \rho A W_n(x)y_o(x)dx. \quad (61)$$

Using the same procedure, the initial modal velocity $\dot{q}_n(0)$ can be related to the actual initial velocity $v_0(x)$ as

$$\dot{q}_n(0) = \frac{1}{\int_0^L \rho A W_n^2(x)dx}\int_0^L \rho A W_n(x)v_o(x)dx. \quad (62)$$

Free vibration. For free vibration, the dynamic response of the passive beam depends only on the initial conditions. Since $F_0 = 0$, the first term in the right-hand side of equation (59) becomes zero. In addition, because the initial velocity $v_0(x)$ is zero, equation (62) and the third term in equation (59) are zero as well.

Thus, the analytical solution for the displacement can be written from equation (52) using the modal displacement equation (59), where the initial modal displacement is given by equation (61)

$$
\begin{aligned}
y(t,x) &= \sum_{n=1}^{\infty} W_n(x)q_n(t) \\
&= \sum_{n=1}^{\infty} W_n(x)\frac{\omega_n}{\omega_{dn}}\frac{1}{\rho A \int_0^L W_n^2(x)dx}
\end{aligned}
\tag{63}
$$

$$
\int_0^L \rho A W_n(x)y_0(x)dx e^{-\zeta_n\omega_n t}\cos(\omega_{dn}t - \psi)
$$

where $\psi = \tan^{-1}(\zeta_n\omega_n/\omega_{dn})$.

Forced vibration. Assume that a concentrated harmonic force $F_d(t) = F_0\sin(\omega_i t)$ is applied at the free end of the cantilever. If the initial conditions for the vertical displacement and velocity are assumed to be zero, then the second and third terms on the right-hand side of equation (59) become zero. Substituting $u(t) = \sin(\omega_i t)$ into equation (59) gives

$$
q_n(t) = \frac{1}{\rho A \int_0^L W_n^2(x)dx}\frac{1}{\omega_{dn}}F_0 W_n(L)
$$

$$
\int_0^t \sin(\omega_i(t-\tau))e^{-\zeta_n\omega_n\tau}\sin\omega_{dn}\tau d\tau.
\tag{64}
$$

The harmonic response of the passive beam in terms of vertical displacement can be calculated from equation (52), for the modal displacement (64), as

$$
\begin{aligned}
y(t,x) &= \sum_{n=1}^{\infty} W_n(x)q_n(t) \\
&= \sum_{n=1}^{\infty} W_n(x)\frac{F_0 W_n(L)}{\rho A \int_0^L W_n^2(x)dx}
\end{aligned}
$$

$$
\frac{1}{\omega_{dn}}\int_0^t \sin(\omega_i(t-\tau))e^{-\zeta_n\omega_n\tau}\sin\omega_{dn}\tau d\tau.
\tag{65}
$$